International Journal of Thermophysics (2025) 46:97
https://doi.org/10.1007/s10765-025-03555-z

Molecular Dynamics Study of the Correlation Between Local Diffusivity of Water Molecules and Ice Nucleation in the Vicinity of a Nanostructured Surface

Shiryu Masuda[1] · Ryosuke Matsumoto[2] · Masahiko Shibahara[1]

Received: 9 March 2025 / Accepted: 9 April 2025

Abstract
The influence of solid surface properties on ice nucleation are well-known and the influence of the dynamical heterogeneity (DH) of water molecules on ice nucleation has also attracted attention recently. Dynamical heterogeneity refers to water molecules in supercooled water that have regions of high mobility as well as those of low mobility. In the present study, we investigated the effect of the dynamic properties of water molecules in the vicinity of various solid surfaces on heterogeneous ice nucleation using molecular dynamics simulations. Specifically, we simulated heterogeneous ice nucleation on a perfect crystalline surface of platinum and surface with a slit structure at a nanometer scale. We calculated the local diffusivity (LD) as an indicator of DH and found that the correlation between the distribution of LD and the location of critical ice nucleation showed that ice nucleation tends to occur in regions with relatively low LD. In addition to this, by employing nanoslit structures of various widths, we found that the surface width of the slit structure or surrounding substrate where ice nucleation occurs is important for critical nucleation.

Keywords Dynamical heterogeneity · Heterogeneous ice nucleation · Molecular dynamics simulation · Nanostructure

✉ Shiryu Masuda
masuda@mte.mech.eng.osaka-u.ac.jp

Ryosuke Matsumoto
matumoto@kansai-u.ac.jp

Masahiko Shibahara
siba@mech.eng.osaka-u.ac.jp

[1] Department of Mechanical Engineering, Osaka University, Suita, Japan

[2] Department of Mechanical Engineering, Kansai University, Suita, Japan

Published online: 13 May 2025

1 Introduction

The formation of frost on heat exchangers is one of the critical problems related to water in industries. Such frost is well-known to be a porous ice layer containing air with low thermal conductivity. Hence, the thermal efficiency of air conditioners and refrigerators is significantly reduced because of increased thermal resistance and pressure loss when frost formation occurs on the heat transfer surfaces [1]. Heat transfer performance of these devices is usually maintained by defrosting with an external heat source or using reverse cycle operations, which requires extra energy consumption. We can expect to reduce excess energy consumption by controlling frost growth artificially. Frost forms when water vapor in the air condenses into droplets on a cooling surface, releasing the supercooled state, and frost crystals develop from the ice droplets. In the control of frost, the freezing process of the supercooled droplets is important. Thus, there are many experimental studies about frost formation or water freezing on solid surfaces. Jhee et al. [2] experimentally investigated the effect of heat exchanger surface treatment on the frosting or defrosting behavior of a fin-tube heat exchanger. Cao et al. [3] studied the icing process of supercooled water on superhydrophobic surfaces and reported its anti-icing function. As a study focusing on the frost itself, Matsumoto et al. [4] measured the microstructure of the frost layer using X-ray microcomputed tomography (μCT).

Supercooling phenomena of liquids such as water also pose problems for the use of phase change materials (PCM). Recently thermal storage technology has become attractive from the viewpoint of effective energy utilization and PCM in particular is capable of high-density heat storage using latent heat. Since PCM utilizes the latent heat of solidification to store and dissipate heat, PCM cannot fully demonstrate its performance under supercooled conditions [5]. Specifically, the instability of thermal storage operation due to supercooling and the increase in cooling costs are issues to be addressed. In both frost control and the use of PCM, the influences of solid surface properties on solidification could be important although the detailed mechanism has not been fully clarified.

It is known that water solidification originates from ice nucleation at molecular scales. Therefore, not only experimental studies but also analysis using molecular dynamics (MD) simulations are effective for understanding the fundamental process of water solidification. Using classical molecular dynamics methods, we can track the behavior of individual molecules in detail by providing potential energy functions for the interactions between atoms and molecules. There are many examples of studies that have applied these methods to the analysis of water solidification and some studies [6–8] have discussed the influence of solid surface properties on water solidification. Martin et al. [6] reported that the wettability and crystal orientation of solid surfaces alter the structural properties of water at the solid–liquid interface and affect the nucleation rate of ice. Li et al. [7] investigated heterogeneous ice nucleation on nano-grooved solid surfaces and reported that the nucleation rate varies with the groove width due to matching with the lattice constant of the ice crystal. Jiang et al. [8] investigated ice nucleation of water

droplets on a solid surface with pillars and reported that the width and height of the pillars affect the ice nucleation rate. These latter results are similar to those of Li's study [7].

As mentioned earlier, there are many studies that have investigated water solidification using molecular dynamics simulations. Among them, researchers reported the relationship between the structural properties of water molecules and heterogeneous ice nucleation. In recent years, the influence of the dynamic properties of water molecules in supercooled water, i.e., the dynamical heterogeneity (DH) [9] of water molecules, on ice nucleation has also been attracting attention. Dynamical heterogeneity is the property which shows spatially separated regions of slow- and fast-moving molecules typically observed in a supercooled liquid. The DH is related to the increase of viscosity of liquid near the glass transition point. Martin et al. [10] investigated homogeneous ice nucleation in bulk supercooled water using dynamical propensity (DP) as an indicator of dynamical heterogeneity and reported that homogeneous ice nucleation is more likely to occur in the relatively low-mobility region. Several studies have further investigated the nucleation of water and other materials using DP. Verde et al. [11] applied DP calculations to several water models and reported correlations with structured water molecules as a preliminary step to crystallization. However, there are still few studies which discuss the relationship between the dynamic properties of supercooled water and ice nucleation, especially the effect of the dynamic properties of water molecules on heterogeneous ice nucleation in systems with a solid–liquid interface. On the other hand, Piero et al. [12] pointed out that analysis using DP is not suitable for comparing DP values between different computational systems. Therefore, Piero et al. [12] investigated the dynamic properties of water molecules at the interface using local diffusivity (LD). They highlighted the significance of LD in assessing the influence of interfaces on the dynamic properties of water molecules and the potential role of LD in heterogeneous ice nucleation They reported that the LD is an alternative indicator to DP to quantify dynamic heterogeneity. Therefore, we performed calculations of LD as defined in Piero's study to investigate the relationships between the dynamic property of water molecules and ice nucleation at solid surfaces of various types.

In the present study, we performed molecular dynamics simulations of heterogeneous ice nucleation and crystallization of water molecules on a solid surface consisting of platinum atoms and investigated the influence of local water molecule dynamics and solid surface properties. To this end we first performed calculations on a solid surface simulating a perfect crystalline surface of platinum. Then we set up various structures on the solid surface and compared them with the perfect crystalline system, especially with respect to ice nucleation on the substrate.

2 Numerical Methods

2.1 Calculation System and Procedure

Figure 1 shows examples of the calculation models for the Pt-H_2O systems used in the present study. We simulated the solidification process of a liquid film composed

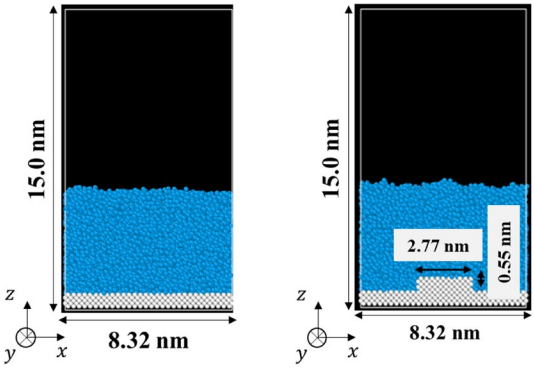

(a) Flat system. (b) Slit system.

Fig. 1 Calculation systems

of water molecules on a solid surface of platinum atoms. Figure 1a and b show calculation systems with the perfect crystalline surface plane of platinum, named as the Flat system and that with a shallow slit structure on a solid surface, named as the Slit system, respectively. In the present study, we refer to the shallow structure shown in Fig. 2 as a slit structure. The slit structure is composed of platinum atoms as well as the solid substrate. The slit structure has a constant size in the x-axis and z-axis directions, and it extends to the periodic boundary length in the y-axis direction. Unless otherwise specified, the snapshots of calculation systems presented hereafter are assumed to be viewed from the same perspective as depicted in Fig. 1. The

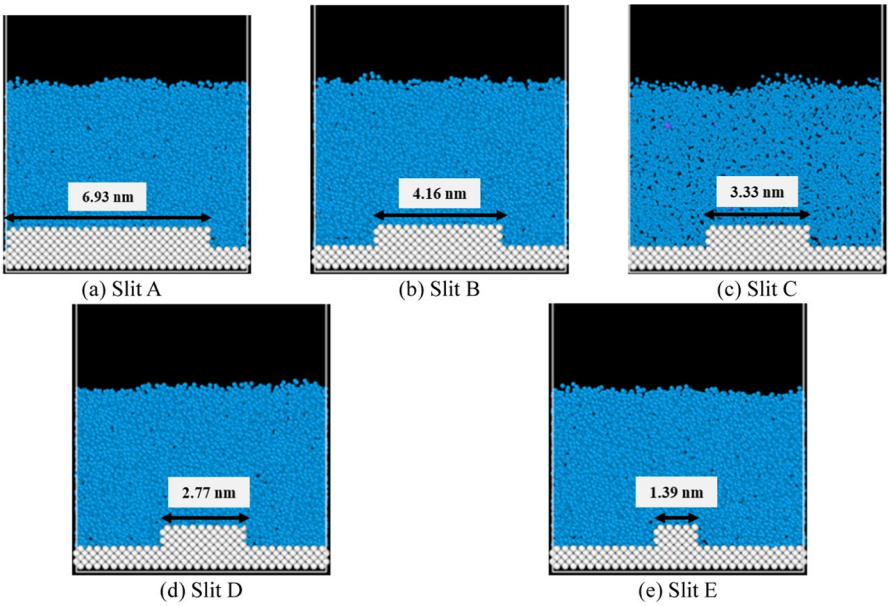

(a) Slit A (b) Slit B (c) Slit C

(d) Slit D (e) Slit E

Fig. 2 Slit systems with various slit widths

dimensions of the computational domain are $x \times y \times z = 8.32 \times 7.85 \times 15.0\text{nm}^3$. Periodic boundary conditions were applied in the x- and y-directions, while a mirror boundary condition was imposed at z = 15.0 nm. The dimensions of the nanoslit structure in the Slit system are $x \times y \times z = W \times 7.85 \times 0.55$. In the present study, the width of the slit structure (W) is changed as described in the following. Therefore, Fig. 1 shows an example of the Slit system while Fig. 2 shows the five different Slit systems employed in the present study. Each system is named as Slit A—Slit E in descending order of the width of the slit structure as 6.93, 4.16, 3.33, 2.77 and 1.39 nm, respectively. The numerical integration of the equations of motion was performed using the velocity-Verlet algorithm with a time step of 5 fs.

We employed the ML-mW model [13] for water molecules. The ML-mW model is an improved version of mW [14], which is a kind of coarse-grained model for a water molecule. The mW model has been widely utilized in the studies of phase transition phenomena due to its accurate reproduction of melting point and structural properties of water [6–8, 10]. The ML-mW model is further improved from mW by fine-tuning its parameters using machine learning, enabling a more accurate representation of the anomalous properties of liquid water. Specifically, the ML-mW model can reproduce the volume expansion during solidification, and the diffusion coefficient is also well simulated. The functional forms of the potential and the corresponding parameters are presented in Eqs. 1, 2, 3, and Table 1, respectively.

$$\phi = \sum_i \sum_{j>i} \varphi_2(r_{ij}) + \sum_i \sum_{j\neq i} \sum_{k>j} \varphi_3(r_{ij}, r_{ik}, \theta_{ijk}) \tag{1}$$

$$\varphi_2(r) = A\varepsilon\left[B\left(\frac{\sigma}{r}\right)^p - \left(\frac{\sigma}{r}\right)^q\right]\exp\left(\frac{\sigma}{r - a\sigma}\right) \tag{2}$$

$$\varphi_3(r, s, \theta) = \lambda\varepsilon\left[\cos\theta - \cos\theta_0\right]^2\exp\left(\frac{\gamma\sigma}{r - a\sigma}\right)\exp\left(\frac{\gamma\sigma}{s - a\sigma}\right) \tag{3}$$

In the present study, we employed the 12–6 Lennard–Jones potential described by Eq. 4 for interactions between platinum atoms, while the interactions between platinum and water were modeled using Eq. 5, scaled by the solid–liquid interaction strength parameter α. The parameters for the Lennard–Jones potential were determined with reference to values from previous studies [13, 15], and the parameters for platinum-water interactions were calculated using the Lorentz-Berthelot mixing rule [16]. The parameters utilized in the present study are summarized in Table 2. For the Flat system, MD simulations were performed with two different values of α,

Table 1 ML-mW model parameters [13]

ε kcal·mol^{-1}	σ nm	a	λ	γ
6.855508	0.1884015	2.124872	24.673877	1.207943
$\cos\theta_0$	A	B	p	q
−0.279667	7.111598	1.991526	4.011214	0.0

Table 2 12–6 Lennard–Jones potential parameters. [14, 16, 17]

	σ nm	ε J
Pt–Pt	0.254	1.09×10^{-19}
Pt–H_2O	0.221	7.21×10^{-20}

0.03 and 0.0475, to model solid surfaces with different wettability. The relationship between the contact angle and α is discussed in Chapter 3. For the Slit system, α was fixed at 0.0475 in the present study.

$$\phi_{ij}(r_{ij}) = 4\varepsilon_{ij}\left\{\left(\frac{\sigma_{ij}}{r_{ij}}\right)^{12} - \left(\frac{\sigma_{ij}}{r_{ij}}\right)^{6}\right\} \tag{4}$$

$$\phi_{ij}(r_{ij}) = 4\alpha\varepsilon_{ij}\left\{\left(\frac{\sigma_{ij}}{r_{ij}}\right)^{12} - \left(\frac{\sigma_{ij}}{r_{ij}}\right)^{6}\right\} \tag{5}$$

For the first 1 ns of the simulation, we controlled the temperature of the water molecules using the velocity scaling method and that of the surface using the Langevin method, maintaining both at 300 K. Following this, we removed the temperature control for the water molecules and performed a relaxation calculation for 4 ns. After the relaxation phase, the controlled temperature of the Pt atoms was adjusted to 246 K, and the main simulation and data collection were conducted for 25–200 ns. Considering that ice nucleation is a spatiotemporally random phenomenon, we performed multiple simulations under identical conditions with different initial velocity distributions: 9 simulations for the Flat system and 15 simulations for the Slit system, respectively. The numbers of average operations were determined considering the convergence of the critical nucleation time for the Flat and Slit systems, respectively. All molecular dynamics simulations were conducted using the LAMMPS software package [17]. For the calculations of crystallization determination and local diffusivity shown in Sects. 2.2 and 2.3, we used our own programs coded with Fortran.

2.2 Determination of Water Molecule Crystallization

We employed the CHILL + algorithm [18] to identify the crystalline state of water molecules. The CHILL + algorithm was introduced to identify water crystals and hydrates, classifying each water molecule into one of four states as Cubic Ice, Hexagonal Ice, Interface, or Liquid, based on the geometric arrangement of neighboring water molecules. Figure 3a, b and c show a snapshot without crystallization identification, a snapshot where crystallization identification was performed using the CHILL + algorithm, and a snapshot where a further ice cluster identification was applied, respectively. In the snapshot in Fig. 3b, particles shown in white represent Pt atoms, while green and red particles correspond to Cubic Ice and Hexagonal Ice,

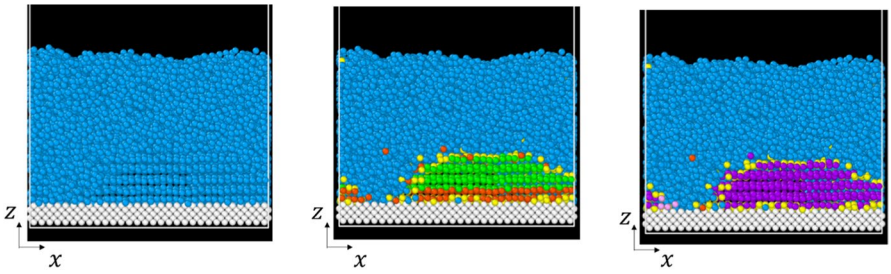

(a) Snapshot (b) Colored by CHILL+ (c) Colored by ice clustering

Fig. 3 Crystallization determination of water molecules. (white: platinum atom, blue: liquid, red: hexagonal ice, green: cubic ice, yellow: interface, light purple: ice cluster, dark purple: the largest ice cluster) (Color figure online)

respectively, indicating water molecules identified as crystallized. Light blue particles represent liquid water molecules (Liquid), and yellow particles denote in intermediate state between crystal and liquid, identified as Interface according to the CHILL + algorithm. To further analyze the behavior of ice nuclei, we performed a clustering analysis of water molecules based on the crystallization identification results from the CHILL + algorithm. For that identification, we utilized the fact that the coordination number of Cubic Ice and Hexagonal Ice is equal to 4 in the CHILL + algorithm [19, 20]. Thus, water molecules identified as Cubic Ice or Hexagonal Ice were considered to be a part of the same ice cluster if one or more of their first to fourth nearest neighbors were also identified as Cubic Ice or Hexagonal Ice. Additionally, since the largest ice cluster in the system is likely to be dominant in determining the progression of crystallization, we distinguished the largest ice cluster from the remaining smaller ice clusters. Figure 3c shows the snapshot after ice cluster identification in the present study. In Fig. 3c, water molecules belonging to the largest ice cluster are shown in dark purple, while those in other ice clusters are shown in light purple. Comparing Fig. 3b to c, the groups of molecules that were colored red or green in Fig. 3b are shown in dark or light purple in Fig. 3c, indicating that the ice cluster identification is reasonable. Figure 3 shows just one example and we have confirmed that the cluster determination is correctly done in all other cases.

2.3 Calculation of Local Diffusivity of Water Molecules

Martin et al. [10] investigated the effect of the dynamic properties of water molecules on ice nucleation using the parameter DP, as expressed in Eq. 6. They reported that homogeneous ice nucleation tends to occur more readily in regions with relatively low mobility. The present study aims to determine whether a similar trend is observed in heterogeneous ice nucleation in calculation systems containing various solid surfaces. However, Piero et al. [12] noted that DP, which is normalized by the mean squared displacement (MSD) of all molecules in the system, is not suitable for comparing DP values across systems with different properties. Considering

this limitation, we employed the parameter LD, as defined in Eq. 7, which does not involve MSD normalization, to investigate the relationship between the dynamic property of water molecules and heterogeneous ice nucleation with varying surface conditions. LD is a quantitative measure of dynamic properties previously used by Piero et al. [12] in their study to investigate water molecular dynamics on carbon surfaces. They highlighted the significance of LD in assessing the influence of interfaces on the dynamic properties of water molecules and their potential role in heterogeneous ice nucleation. LD shows the similar physical meaning as self-diffusion coefficient of one water molecule. However, as shown in Eq. 7, LD is an indicator of the non-dimensionalized dynamical heterogeneity of the molecule during t_0 which is different from the characteristic time of usual self-diffusion coefficient. Both Eqs. 6 and 7 involve fixing the initial molecular configuration and assigning random initial velocities to molecules based on the Maxwell–Boltzmann distribution. This approach is named ISOCA (iso-configurational analysis) [21]. Fluctuations due to the initial configuration can be eliminated using the ISOCA, where $\langle\rangle_{\mathrm{ISO}}$ denotes an ensemble average over initial velocities. However, the ISOCA method requires high computational costs, and it is difficult to apply in the time transient analysis. Therefore, we redefined LD in a time-dependent form, as shown in Eq. 8, to account for temporal variations of LD. Here, $\boldsymbol{r}_i(t)$ represents the position vector of a water molecule at time t, $\sigma_{\mathrm{H_2O}}$ is a parameter representing the apparent particle diameter in the ML-mW model, and t_0 is the time at which the dynamic heterogeneity [9] of the molecules is maximized. From preliminary calculations according to the following procedure[10], t_0 was determined to be 1.08 ps in the present study. The isotropic structure factor $S(q)$ can be calculated using Eq. 9. Here, ρ is the liquid density, $g(r)$ is the radial distribution function. We define q_0 as the value where $S(q)$ has its first peak, with q being a reciprocal length. For this q_0, we calculate the quantity $\Phi(\mathbf{q},t)$ using Eq. 10. Via $\Phi(\mathbf{q},t)$, we can obtain the self-intermediate scattering function $\langle\Phi(\mathbf{q},t)\rangle$ and the dynamical susceptibility $\chi_4(\mathbf{q},t)$ can be calculated using Eq. 11. The time of maximum heterogeneity t_0 is taken as the time where $\chi_4(\mathbf{q},t)$ has its maximum.

$$\mathrm{DP}_i = \langle \frac{\|\boldsymbol{r}_i(t_0) - \boldsymbol{r}_i(0)\|^2}{\mathrm{MSD}} \rangle_{\mathrm{ISO}} \tag{6}$$

$$\mathrm{LD}_i = \frac{\langle \|\boldsymbol{r}_i(t_0) - \boldsymbol{r}_i(0)\| \rangle_{\mathrm{ISO}}}{\sigma_{\mathrm{H_2O}}} \tag{7}$$

$$\mathrm{LD}_i(t) = \frac{\|\boldsymbol{r}_i(t+t_0) - \boldsymbol{r}_i(t)\|}{\sigma_{\mathrm{H_2O}}} \tag{8}$$

$$S(q) = 1 + \frac{4\pi\rho}{q} \int_0^\infty r \sin(rq)\big[g(r) - 1\big]\mathrm{d}r \tag{9}$$

$$\Phi(\mathbf{q},t)=\frac{1}{N}\sum_{j=1}^{N}\exp\left(i\mathbf{q}\cdot\left[\mathbf{r}_j(t)-\mathbf{r}_j(0)\right]\right) \tag{10}$$

$$\chi_4(\mathbf{q},t)=N\left[\langle|\Phi(\mathbf{q},t)|^2\rangle-\langle\Phi(\mathbf{q},t)\rangle^2\right] \tag{11}$$

3 Results and Discussion

3.1 Ice Nucleation in the Flat system

To investigate the ice nucleation on the Flat surface under different wettability conditions, we varied the solid–liquid interaction strength α of the 12–6 Lennard–Jones potential between platinum and water in two ways, one with α = 0.0475, representing weak hydrophilicity, and another with α = 0.03, representing weak hydrophobicity. The contact angles were measured as 80.2 and 110.4 degrees as shown in Fig. 4, respectively, which illustrates the wetting behavior of liquid water columns on the Pt solid surfaces under each condition. The system with α = 0.0475 is referred to as the hydrophilic system, while the other system with α = 0.03 is referred to as the hydrophobic system for qualitative discussion here.

Figure 5 shows an example of the crystallization process in the Flat system. Under the conditions used in the present study, crystallization consistently initiated near the solid surface in all simulations, suggesting that heterogeneous ice nucleation occurred preferentially. The critical nucleus size was defined based on prior studies [22, 23] as the point at which the largest ice cluster size, that is, the number of water molecules in the largest ice cluster, began to grow irreversibly. In the present simulations, once the largest ice cluster size exceeded 50 molecules, the crystallization proceeded without the disappearance of the ice nucleus. Therefore, we defined the critical nucleus formation time as the moment when the largest ice cluster size firstly

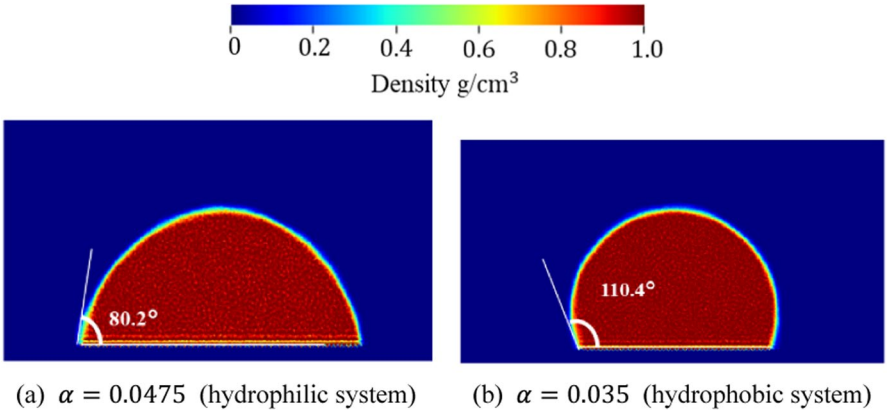

Fig. 4 Contact angle of a water column and α on each surface

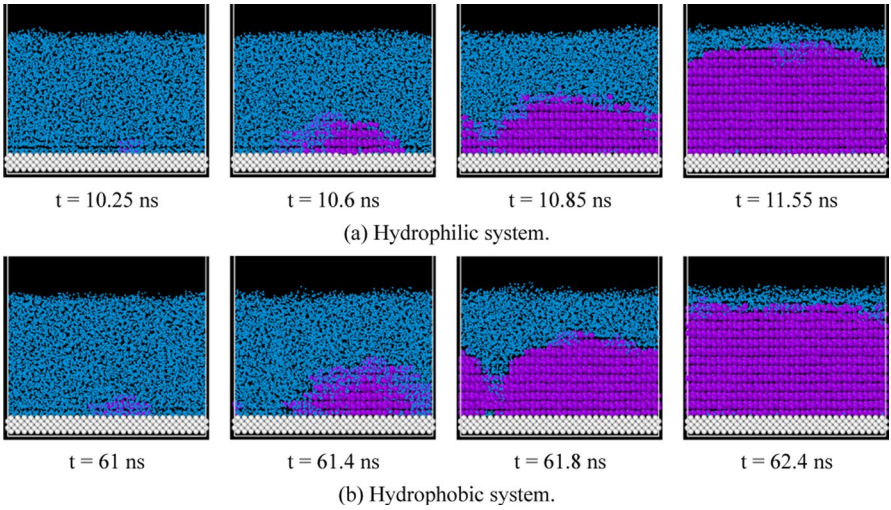

Fig. 5 Visualization of crystallization process in flat systems

exceeded 50 molecules. Table 3 summarizes the critical nucleus formation times for nine simulations with different initial velocity distributions for each system. The average critical nucleus formation time were calculated as 5.6 ns for the hydrophilic system and 105.7 ns for the hydrophobic system, respectively, indicating that the crystallization proceeded more slowly under lower wettability conditions [24].

Figure 6 shows the distributions of LD and density along the z-axis direction in the supercooled state. This data represents the average values obtained from nine cases with different initial velocity distributions for both the hydrophilic and hydrophobic Flat systems. In Fig. 6, we plot the data averaged over 0.3 ns just before the onset of water molecule crystallization. We discuss the determination of the 0.3 ns period in detail in Fig. 7. With increasing z coordinate, the LD

Table 3 Critical nucleation time in flat systems

	Hydrophilic system (ns)	Hydrophobic system (ns)
Case 1	10.4	29.4
Case 2	6.6	162.2
Case 3	2.7	155.8
Case 4	3.2	68.9
Case 5	3.0	94.0
Case 6	8.4	186.9
Case 7	8.3	165.0
Case 8	4.4	28.5
Case 9	3.3	61.0
Average	5.6	105.7
Standard deviation	2.7	58.8

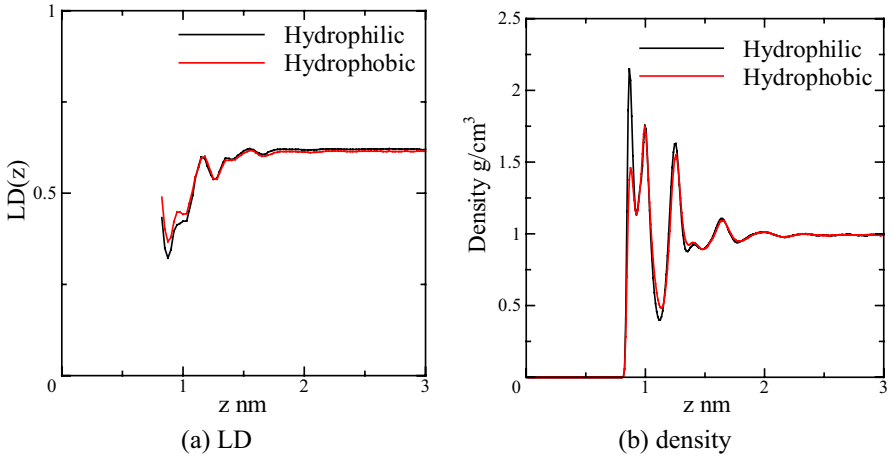

Fig. 6 LD and density distribution along z direction in supercooled state of water in flat systems

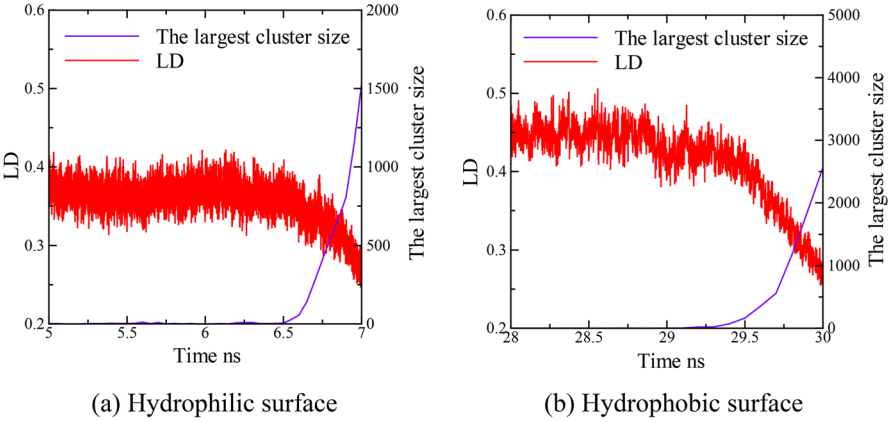

Fig. 7 Time transitions of LD in the vicinity of a solid surface and the largest cluster size

values exhibit an oscillatory increase near the solid surface, eventually reaching a constant value in regions at z > 2.0 nm, where they are unaffected by the solid surface. In the hydrophobic system, in which the surface wettability is relatively low, the LD values near the solid surface are larger compared to the hydrophilic system. This is likely due to the reduced adsorption of water molecules onto the solid surface in the hydrophobic case as shown by the lower density of the red curve in Fig. 6b. Additionally, the first peak of LD near the solid surface shows a negative correlation with the peak of the density distribution. This is because the water molecules are prevented from moving due to the effect of adsorption on the solid surface where the density peak is relatively high.

Figure 7 shows the temporal changes in the largest ice cluster size and the LD near the solid surface (z < 1.1 nm) before and after the onset of crystallization at 6.5(Fig. 7a) and 29.1(Fig. 7b) ns in the case of hydrophilic and hydrophobic surfaces, respectively. Although Fig. 7 presents a representative case among the nine simulations performed under different initial conditions for each system, similar trends were observed in all other cases, as discussed later. In Fig. 7, while the LD values fluctuate significantly near the solid surface, they tend to decrease as the ice nucleus grows. Additionally, it is evident that the LD values exhibit a decreasing trend approximately 0.3 ns before the onset of crystallization at 6.5 (Fig. 7a), 29.1 (Fig. 7b) ns during the supercooled state, respectively. These periods from 6.2 ns to 6.5 ns in Fig. 7a, for example, correspond to the dynamic latent period described in the study by Martin et al. [8]. In the present study, for each system with various initial conditions, we used the data from the 0.3 ns immediately preceding the onset of crystallization to create two-dimensional LD distributions in the xy-plane near the solid surface (z < 1.1 nm). Figure 8 shows an example of the two-dimensional

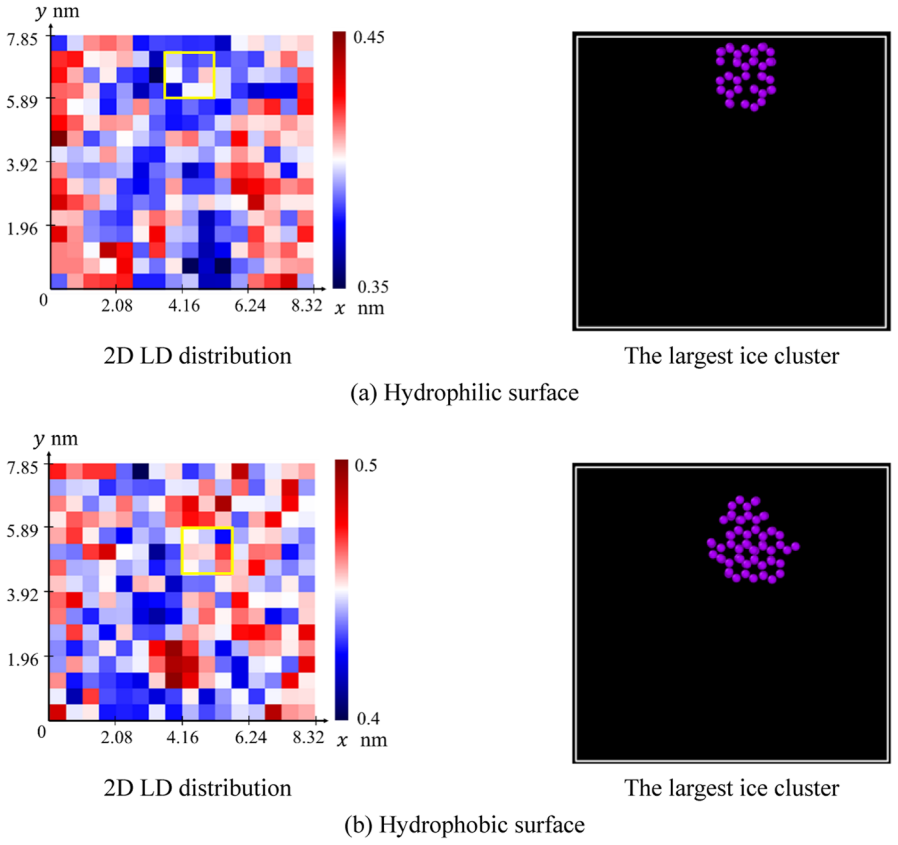

Fig. 8 2D LD distribution in the vicinity of a solid surface and the snapshot of the largest ice cluster in Flat systems in supercooled state of water

LD distribution near the solid surface ($z < 1.1$ nm) and the visualization of the largest ice cluster in the system for each simulation case. The region enclosed in yellow on the two-dimensional distribution of LD corresponds to the locations of critical nucleus formation, which is the region centered on the center of gravity of the critical nucleus. For all nine simulation results under different initial conditions, we investigated whether there was a correlation between the locations of critical nucleus formation and the magnitude of LD. To clarify the relationship between the dynamic properties of water molecules and the critical nucleus formation locations, we calculated the percentile ranking of the average LD of the $3 \times 3 = 9$ regions corresponding to the critical nucleus formation locations, out of all $16 \times 16 = 256$ regions in the two-dimensional distribution, considering the fluctuation of the center of mass of ice nucleus growth. The results of the nine simulations with different initial velocity distributions for each system are shown in Table 4. If the critical nucleus formation locations were to occur randomly and independently of LD, the average of many sampled nucleus formation locations would approach 50 %. However, in the hydrophilic and hydrophobic systems employed, the average values were 35 % and 18 %, respectively, indicating that critical nuclei tended to form in regions with relatively low LD values. This suggests that the dynamic properties of water molecules in the supercooled state influence heterogeneous ice nucleation near the atomically smooth surface. The stronger manifestation of this trend in the hydrophobic system can be attributed to the higher LD values near the solid surface compared to the hydrophilic system due to lower wettability.

3.2 Ice Nucleation in the Slit System

In the Slit system employed in the present study, the solid–liquid interaction strength is set to $\alpha = 0.0475$, which is the same value as in the hydrophilic system of the Flat configuration. This section is divided into two parts: in the first part, the results concerning the LD and critical nucleus formation locations in the Slit system are presented; in the second part, the effects of slit structure size

Table 4 Correlation between LD in the vicinity of a solid surface and critical nucleation position

	Hydrophilic (%)	Hydrophobic (%)
Case 1	37.3	7.8
Case 2	15.7	15.3
Case 3	16.5	2.4
Case 4	20.8	14.5
Case 5	34.1	1.6
Case 6	57.6	1.6
Case 7	39.6	24.7
Case 8	58.0	36.9
Case 9	35.3	57.3
average	35.0	18.0
Standard deviation	14.9	17.8

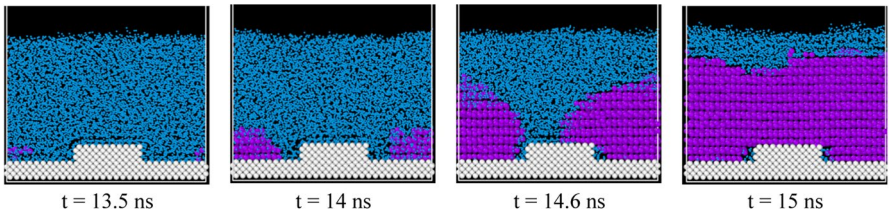

Fig. 9 Visualization of crystallization process in Slit D

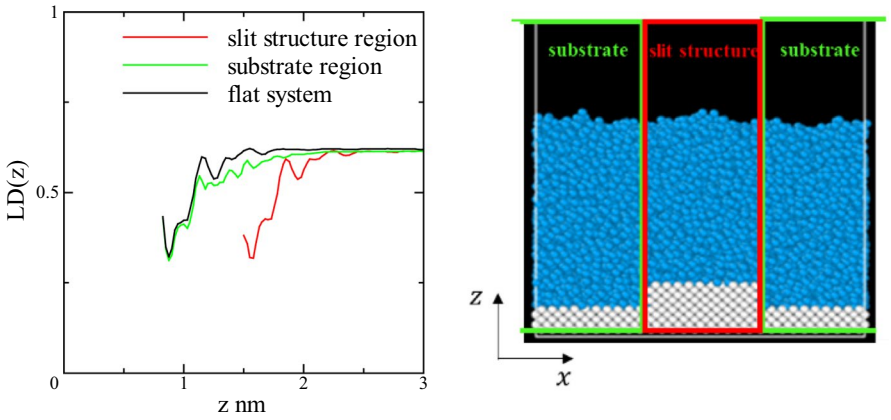

(a) LD distribution (b) definition of each area

Fig. 10 LD distribution along the z direction in supercooled state in Slit D. "substrate" and "slit structure" in left figure (a). correspond to the surfaces in the right figure (b)

on critical nucleus formation are investigated. The discussion in the first part is based on the Slit D shown in Fig. 2.

Figure 9 shows an example of the crystallization process in the Slit D. In all 15 simulations with different initial velocity distributions conducted in the present study, the critical nucleus formed while avoiding the side walls of the slit structure located at the center of the substrate, as shown in Fig. 9. The average crystallization onset time was 45.5 ns, which is longer than the hydrophilic Flat system but shorter than the hydrophobic Flat system described in Sect. 3.1. The longer crystallization time compared to the hydrophilic Flat system with similar wettability α suggests that the slit structure has the effect of inhibiting ice nucleation under the present conditions.

As in the case of the Flat systems, the LD of water molecules was also investigated for the Slit D. Figure 10 shows the LD distribution along the z-axis in the supercooled state. In the Slit D, in order to determine the LD distribution along the z direction, the surface was divided into two regions, that just above the slit structure and that just above the substrate, respectively, as shown in Fig. 10b. The LD distribution was calculated for each region of the slit structure and the

substrate. In Fig. 10a, we averaged the data during 0.3 ns for the Slit D as for the Flat systems, just before the start of crystallization. Figure 10a displays the LD distribution for each region, along with the LD distribution of the hydrophilic Flat system for comparison. The LD distribution is the average of 15 calculations with different initial condition. The shape of LD distributions along the z-axis are generally similar to those observed in the Flat system. However, in the region directly above the substrate, the LD values near the solid surface are lower than those of hydrophilic Flat system. This is likely due to the effects of molecular adsorption originating from the side surfaces of the slit structure.

Next, we examine the two-dimensional LD distribution near the solid surface in Slit D. Considering that no critical nucleus generation was observed on the slit structure under the current conditions in the case of the Slit D, a two-dimensional LD distribution was constructed only above the substrate, as shown in Fig. 11. To draw the 2D LD distribution, we calculated LD during 0.3 ns just before the onset of crystallization in the region $z < 1.1$ nm as in the Flat system. The dark blue region in the range approximately from 2.6 nm to 5.7 nm in the x-axis, corresponds to the region where water molecules are excluded due to the presence of the slit structure. Furthermore, in areas close to the side surfaces of the slit structure, the LD values are extremely low due to the adsorption of water molecules on the side surfaces. Based on this, the yellow-outlined region in Fig. 11, consisting of $8 \times 16 = 128$ regions, was selected for the following analysis. Using the same method as in the Flat system, the correlation between the critical nucleus generation sites and the LD distribution was investigated. The results from 15 simulations are summarized in Table 5. The average correlation value was 41.8 %, indicating that critical nucleus tends to form in relatively low-mobility regions. However, compared to the Flat system, this tendency was less pronounced. In the Flat system, the positional relationship between water molecules and the solid surface was equivalent across all planar positions. In contrast, the structural characteristics of water molecules in Slit D varied depending on the distance from the side walls of the slit structure. This structural variation likely reduced the influence of LD on the critical ice nucleation in the case of the Slit systems.

To further investigate the impact of the presence of the slit structure, the MD calculations were performed using Slit systems with structures having various slit widths where the overall system size and slit height were not changed. The Slit

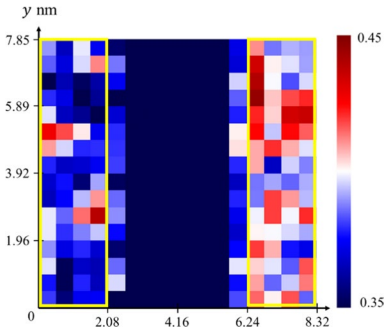

Fig. 11 2D LD distribution in the vicinity of a solid surface in Slit D. (The yellow-outlined region, excluding the area with extremely small LD due to adsorption on the slit structure, is the target of analysis.)

Table 5 Correlation between LD in the vicinity of a solid surface and critical nucleation position in Slit D

Case 1	75.6 %
Case 2	14.2 %
Case 3	77.2 %
Case 4	34.6 %
Case 5	47.2 %
Case 6	22.0 %
Case 7	34.6 %
Case 8	35.4 %
Case 9	76.4 %
Case 10	57.5 %
Case 11	48.8 %
Case 12	11.0 %
Case 13	7.9 %
Case 14	23.6 %
Case 15	61.4 %
Average	41.8 %
Standard deviation	23.1 %

systems employed are shown in Fig. 2. Table 6 provides detailed specifications for each Slit system. From left to right in the table, the columns indicate the x-axis length of the slit structure, the x-axis length of the substrate without the slit structure, the proportion of critical nucleation on the slit structure in the total 15 calculations, the proportion of critical nucleation on the substrate in the total 15 calculations, and the average time for critical ice nucleation. The critical ice nucleation times for each Slit system were determined from 15 calculations using different initial velocity distributions, and the results are summarized in Table 7. As shown in Table 6, the size of the slit structure influenced the location of critical nucleus formation, that is, whether they were formed on the slit structure or on the substrate. Moreover, the results for Slit A and Slit E showed significantly shorter critical nucleus formation times compared to the other three Slit systems. In the present study, the size of the entire calculation system and the height of the slit structure are fixed, so the x-axis width of the slit structure and substrate are considered essential

Table 6 Details of slit systems A–E

	Width of slit structure nm	Bottom width of substrate nm	Proportion of critical nucleation on the structure	Proportion of critical nucleation on the substrate	Average time of critical nucleation ns
Slit A	6.93	1.39	1.00	0.00	23.5
Slit B	4.16	4.16	0.73	0.27	56.8
Slit C	3.33	4.99	0.07	0.93	55.5
Slit D	2.77	5.55	0.00	1.00	45.5
Slit E	1.39	6.93	0.00	1.00	21.9

Table 7 Critical nucleation time in slit systems A–E: the unit is ns

	Slit A	Slit B	Slit C	Slit D	Slit E
Case 1	34.2	33.8	42.2	13.8	4.0
Case 2	2.6	157.0	7.0	16.1	22.0
Case 3	25.7	126.8	6.8	67.7	2.5
Case 4	55.2	16.4	13.3	38.9	15.7
Case 5	2.7	35.3	74.8	61.4	35.5
Case 6	37.8	88.6	39.4	43.6	4.1
Case 7	8.8	42.8	5.0	8.5	6.9
Case 8	47.9	3.1	82.1	61.8	53.4
Case 9	6.0	36.9	14.5	44.8	43.7
Case 10	6.7	38.9	129.4	20.5	34.2
Case 11	1.5	38.0	22.5	121.4	22.1
Case 12	20.3	20.4	187.8	28.4	29.5
Case 13	15.1	26.4	80.9	5.3	41.3
Case 14	53.3	54.0	125.2	6.6	1.3
Case 15	35.3	134.0	2.0	143.0	12.9
Average	23.5	56.8	55.5	45.5	21.9
Standard deviation	18.6	45.4	54.6	39.7	16.4

for the location of the critical nucleation. This indicates that when either the slit structure or the substrate is relatively large, the critical nucleus formation is more likely to occur just above them. The present trend suggests that the spatial configuration of the solid–liquid interface, that is the planar width of the slit structure or the substrate here, plays a crucial role in facilitating or inhibiting ice nucleation. A larger x-axis width, whether in the slit or the substrate, may create conditions that promote the onset of crystallization, potentially by modifying the dynamic and structural properties of the water molecules near the interface.

Figure 12 shows the correlation between the x-axis length of the slit structure or substrate without the slit structure and the average time for critical ice nucleation. Here, the critical ice nucleation times were averaged for those formed on the substrate and those on the structure separately, that is, distinct from the values presented in Table 3. For comparison, the results for the Flat system were plotted using the x-axis periodic boundary length of the system. From this figure, it is evident that the larger width area available for ice nucleus growth, the shorter the time required for the critical nucleus formation. This is likely because, in regions with a smaller x-axis width, the ice nucleus growth in that direction is hindered, leading to frequent disappearance of nuclei before reaching the critical size. To confirm this qualitatively, Fig. 13 illustrates examples of the growth of the largest ice cluster in the Slit systems. Figure 13a presents an example in Slit C, while Fig. 13b provides an example in Slit D. Ice nuclei whose growth along the x-axis seemed to be inhibited grew into clusters with approximately 40 molecules, as shown in Fig. 13a. These clusters maintain their state as ice nuclei for a certain period before eventually vanishing. In contrast, as shown in Fig. 13b, critical nuclei rapidly grew after exceeding the ice cluster size of approximately 50 molecules. Using this value as the definition of

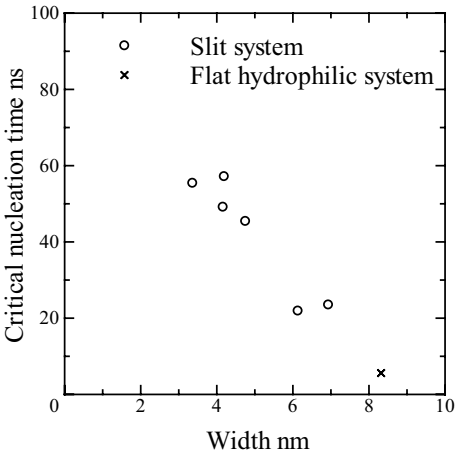

Fig. 12 Correlation between the length of the slit structure or a substrate without the slit structure in x-direction and critical nucleation time

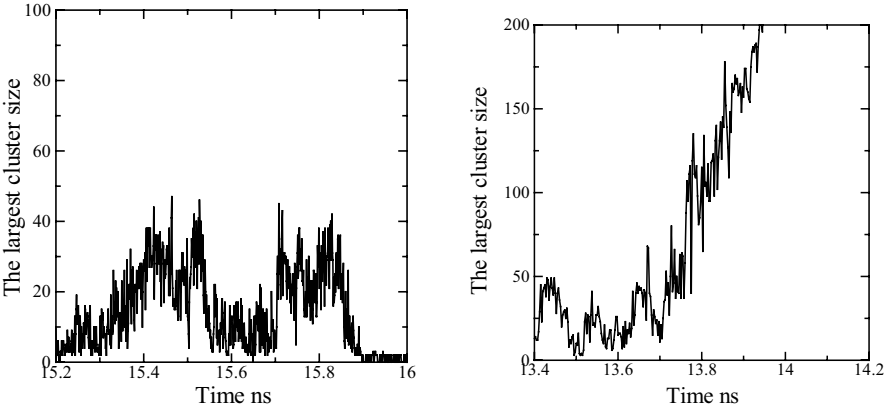

(a) extinction of ice nucleus. (b) critical ice nucleation and growth

Fig. 13 Comparison of ice cluster size growth of a critical ice nucleus and a nucleus that did not grow to criticality

critical nucleus, whether the ice nucleus can grow to the size of 50 molecules significantly influences the subsequent growth behavior of the nucleus. System snapshots corresponding to the period in Fig. 13a and b are shown in Figs. 14 and 15, respectively. In Fig. 14, only water molecules identified as parts of ice clusters of interest are displayed to clearly indicate the ice cluster positions. At the time when the ice nucleus grew to approximately 40 molecules, as shown in Fig. 14, the ice nucleus expanded to nearly the edges of the slit structure. In the case of Fig. 15, when the ice nucleus grew to the sides of the slit structure, there was likely to be inhibition of growth in x-axis direction but before that happened the ice nucleus had reached the critical size. Similar phenomena shown in Fig. 13a could be observed in other cases and we believe the inference that the ice nuclei are restricted and cannot

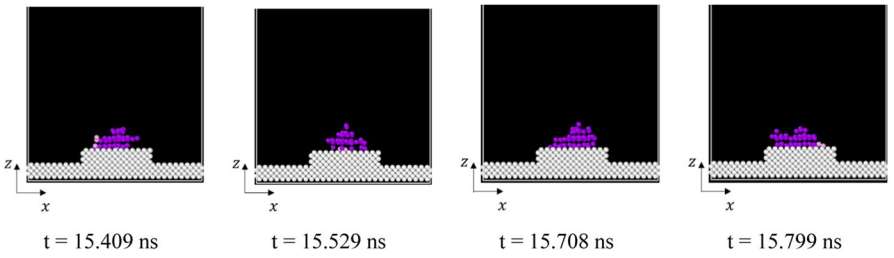

Fig. 14 Visualization of an ice nucleus that did not reach the critical size

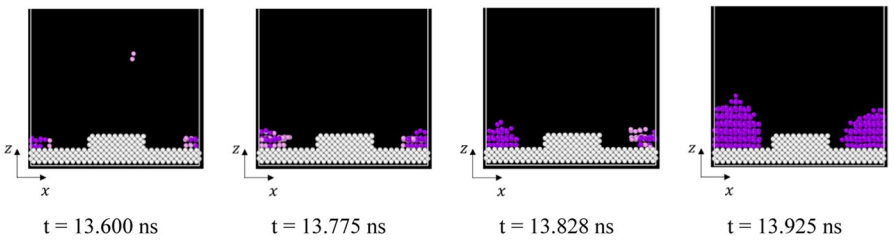

Fig. 15 Visualization of an ice nucleus that reached the critical size

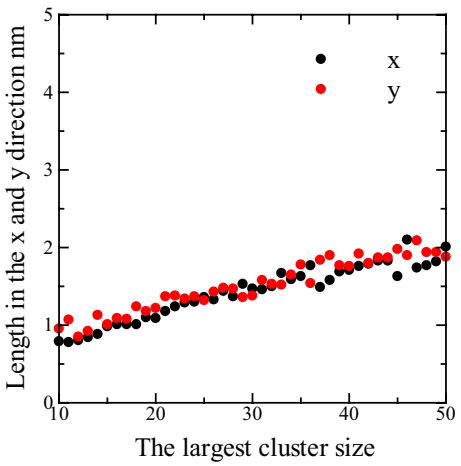

Fig. 16 Influence of the water cluster size on its length in the x and y directions in the system of Slit D. Cluster size represents the number of water molecules in the cluster

grow to a critical size is one of the reasons that the length of the flat region of the slit or substrate in the x-direction has the strong correlation with the critical nucleation time shown qualitatively in Fig. 12. In Fig. 16, we have examined the influence of the water cluster size on its lengths in the x and y directions in the system of Slit D averaged over 15 cases. Figure 16 shows that the average size of the critical nucleus is about 2 nm when the cluster size corresponds to 50 water molecules. Considering the influence of the sides of slit structures, the average critical nucleus size of 2 nm

is reasonable to explain the inhibition of cluster growth by the size of the slit structures in the x-direction.

4 Conclusions

In the present study, we visualized heterogeneous ice nucleation near solid surfaces using molecular dynamics simulations and investigated the dynamic properties of water molecules near platinum solid surfaces using LD, as well as the impact of rectangular slit structures on heterogeneous ice nucleation. The ML-mW potential was employed for the water molecule potential function, and the CHILL + algorithm was used to identify crystallization. The main findings obtained in the present study are summarized below.

Under the conditions employed, critical nucleus formation near solid surfaces was observed in the Flat system, which simulates a perfectly crystalline Pt surface, for both interaction strengths $\alpha = 0.0475$ and $\alpha = 0.03$ corresponding to contact angles of 80.2 and 110.4 degrees, respectively. A comparison of the two-dimensional LD distributions of water molecules in the xy-plane and the positions of critical nucleus formation revealed that, in Flat systems with different wettability, the critical nucleus tended to form in regions with relatively low LD. This tendency was particularly pronounced in the $\alpha = 0.03$ system, which exhibits lower wetting. Furthermore, these results are consistent with findings by Martin et al. in their previous study, which demonstrated similar trends for homogeneous ice nucleation in bulk water systems. The present study extends these observations to systems involving solid surfaces employing LD instead of DP.

Regarding heterogeneous ice nucleation in the Slit system, where a slit structure with a width of one-third of the x-axis periodic boundary length, which corresponds to 2.77 nm, was introduced, the critical nucleus formation was limited to the substrate surfaces. No critical nucleus formation was observed above the slit structure itself. Additionally, even on the substrate, the critical nuclei tended to form at locations relatively distant from the slit structure. Considering these results, a two-dimensional LD distribution was calculated for water molecules near the solid substrate, and its correlation with critical nucleus formation positions was examined, as was done for the Flat system. While critical nuclei still tended to form in regions with relatively low mobility, this tendency was less pronounced compared to the Flat system with similar wetting properties. These observations suggest that the influence of the LD of water molecules on the critical nucleus formation positions is weaker in the Slit system than in the Flat system.

To further investigate the influence of a slit structure on critical nucleus formation, we conducted simulations using the Slit system when the width of the calculation system and the height of the slit structure were fixed and the width of the slit structure varied. The results revealed that the critical nucleus formation time was shorter in systems with either extremely large or extremely small slit widths within the limitation of the present system size, which implies the inhibition of ice nucleation at sufficient small space between slit structures compared with the size of the critical nucleus. Additionally, the average nucleation time was calculated separately

for critical nuclei formed on the substrate and those formed on the slit structure for each Slit system. The average nucleation time and the width of the respective regions, for the substrate or the slit structure, showed a clear negative correlation. This indicates that the width in the x-axis direction available for ice nucleus growth significantly influences the critical nucleation time. The difficulty in forming critical nuclei on relatively narrow surfaces can be attributed to the restriction imposed by the width in the x-axis direction, which hinders the growth of ice nuclei to the critical size.

The results of the present study demonstrate the significant influence of the dynamic properties of water molecules on heterogeneous ice nucleation on solid surfaces. Furthermore, we have examined the correlation between the width of the slit structure and the position and timing of critical nucleus formation.

Author Contributions S.M. conducted MD simulations and prepared all figures and tables. S. M. and M. S. conducted data analysis and wrote the original draft. R. M. and M. S. supervised the present research. All authors contributed to the conceptualization and reviewed the manuscript.

Funding Open Access funding provided by The University of Osaka. This work was supported by the Japan Society for the Promotion of Science (JSPS), Grant-in-Aid for Science Research No. 23H01355.

Data Availability No datasets were generated or analysed during the current study.

Declarations

Conflict of interest The authors declare no competing interests.

References

1. M. Song, C. Dang, Int. J. Heat Mass Transf. **124**, 586–614 (2018). https://doi.org/10.1016/j.ijheatmasstransfer.2018.03.094
2. S. Jhee, K. Lee, W. Kim, Int. J. Refrig. **25**, 1047–1053 (2002). https://doi.org/10.1016/S0140-7007(02)00008-7
3. L. Cao, A.K. Jones, V.K. Sikka, J. Wu, D. Gao, Langmuir **25**, 12444–12448 (2009). https://doi.org/10.1021/la902882b
4. R. Matsumoto, T. Uechi, Y. Nagasawa, J. Therm. Sci. Technol. **13**, 1 (2018). https://doi.org/10.1299/jtst.2018jtst0014
5. I. Shamseddine, F. Pennec, P. Biwole, F. Fardoun, Renew. Sustain. Energy Rev. **158**, 112172 (2022). https://doi.org/10.1016/j.rser.2022.112172
6. M. Fitzner, G.C. Sosso, S.J. Cox, A. Michaelides, J. Am. Chem. Soc. **137**, 13658–13669 (2015). https://doi.org/10.1021/jacs.5b08748

7. C. Li, R. Tao, S. Luo, X. Gao, K. Zhang, Z. Li, J. Phys. Chem. C **122**, 25992–25998 (2018). https://doi.org/10.1021/acs.jpcc.8b07779
8. J. Jiang, G.X. Li, Q. Sheng, G.H. Tang, Appl. Surf. Sci. **510**, 145520 (2020). https://doi.org/10.1016/j.apsusc.2020.145520
9. M.D. Ediger, Annu. Rev. Phys. Chem. **51**, 99–128 (2000). https://doi.org/10.1146/annurev.physchem.51.1.99
10. M. Fitzner, G.C. Sosso, S.J. Cox, A. Michaelides, The. Proceed. Nat. Acad. Sci. **116**, 2009–2014 (2019). https://doi.org/10.1073/pnas.1817135116
11. A.R. Verde, J.M.M. Oca, S.R. Accordino, L.M. Alarcon, G.A. Appignanesi, J. Chem. Phys. **150**, 244504 (2019). https://doi.org/10.1063/1.5108796
12. P. Gasparotto, M. Fitzner, S.J. Cox, G.C. Sosso, A. Michaelides, Nanoscale **14**, 4254–4262 (2022). https://doi.org/10.1039/D2NR00387B
13. H. Chan, M.J. Cherukara, B. Narayanan, T.D. Loeffler, C. Benmore, S.K. Gray, S.K.R.S. Sankaranarayanan, Nat. Commun. **10**, 379 (2019). https://doi.org/10.1038/s41467-018-08222-6
14. V. Molinero, E.B. Moore, J. Phys. Chem. B **113**, 4008–4016 (2009). https://doi.org/10.1021/jp805227c
15. S. Zhu, M.R. Philpott, J. Chem. Phys. **100**, 6961–6968 (1994). https://doi.org/10.1063/1.467012
16. D. Boda, D. Henderson, Mol. Phys. **106**, 2367–2370 (2008). https://doi.org/10.1080/00268970802471137
17. S. Plimpton, J. Comput. Phys. **117**, 1–19 (1995). https://doi.org/10.1006/jcph.1995.1039
18. A.H. Nguyen, V. Molinero, J. Phys. Chem. B **119**, 9369–9376 (2015). https://doi.org/10.1021/jp510289t
19. N.D. Lisgarten, M. Blackman, Nature **178**, 39–40 (1956). https://doi.org/10.1038/178039a0
20. J.D. Bernal, R.H. Fowler, J. Chem. Phys. **1**, 515–548 (1993). https://doi.org/10.1063/1.1749327
21. A. Widmer-Cooper, P. Harrowell, J. Chem. Phys. **126**, 154503 (2007). https://doi.org/10.1063/1.2719192
22. L. Lupi, A. Hudait, V. Molinero, J. Am. Chem. Soc. **136**, 3156–3164 (2014). https://doi.org/10.1021/ja411507a
23. Q. Xu, H. Wang, J. Wu, Z. Zhang, Cryst. Growth Des. **21**, 4354–4361 (2021). https://doi.org/10.1021/acs.cgd.1c00253
24. Y. Ueki, Y. Tsutsumi, M. Shibahara, Int. J. Heat Mass Transfer. **194**, 123004 (2022). https://doi.org/10.1016/j.ijheatmasstransfer.2022.123004